

# Chemical Vapor Deposition Growth and Characterization of ReSe<sub>2</sub>

J. Onasanya<sup>b)1</sup>, Mourad Benamara<sup>2</sup>, Kanagaraj Moorthi<sup>2</sup>, H. O. H. Churchill<sup>1,2,3</sup>, Bothina

Hamad<sup>a), 1,3</sup>, M. O. Manasreh<sup>1,4</sup>

<sup>1</sup>Materials Science and Engineering, University of Arkansas, Fayetteville, AR 72701, USA

<sup>2</sup>Institute for Nanoscale Science and Engineering, University of Arkansas, Fayetteville, AR 72701

<sup>3</sup>Department of Physics, University of Arkansas, Fayetteville, AR 72701, USA

<sup>4</sup>Department of Electrical Engineering and Computer Science, University of Arkansas, Fayetteville, AR 72701, USA

## Abstract

Two-dimensional (2D) flakes of ReSe<sub>2</sub> structure were grown by chemical vapor deposition and investigated at room temperature using Raman, photoluminescence, and absorption spectroscopies. The Raman spectra revealed eighteen phonon modes in the range of 100-300 cm<sup>-1</sup> that were found in good agreement with the density functional theory (DFT) calculations. The thickness profiles of the ReSe<sub>2</sub> flakes are in the range of 5-50 nm. The ReSe<sub>2</sub> crystal structure and morphology were investigated using XRD, atomic force microscopy and scanning electron microscopy. The energy dispersion spectroscopy confirmed the 1:2 elemental composition. The absorption spectra were obtained for ReSe<sub>2</sub> flakes and found to exhibit excitonic peaks in the spectral region of 885 - 942 nm (1.401 – 1.316 eV). These peaks are used to define the band gap of the material. The DFT calculations predicted an indirect bandgap of 0.88 eV for the bulk structure, while a direct bandgap of 1.26 eV was predicted for the monolayer.

*Keywords:* ReSe<sub>2</sub>, absorbance, DFT, phonons, Raman

<sup>a)</sup>Email of corresponding authors: [bothinah@uark.edu](mailto:bothinah@uark.edu)

<sup>b)</sup>Email of corresponding authors: [onasanya@uark.edu](mailto:onasanya@uark.edu)

## 1. Introduction

Two-dimensional (2D) chalcogenide materials have attracted considerable interest due to their strong in-plane covalent bonds that contrasted with the weak van der Waals interlayer bonds. This van der Waals properties allow easy mechanical exfoliation at the atomic level where electron confinement plays a major role [1-3]. This crystallographic nature leads to intriguing electrical and optoelectronic device characteristics, such as carrier mobility, exciton binding energy, phonon scattering, and thermal conductivity [4-10]. Among these 2D materials, there is an emerging class of low-symmetry materials with orthorhombic, monoclinic, or triclinic crystal structures with unique in-plane lattice arrangements that leads to in-plane orientation-dependent physical properties [11-14]. The distinct properties of these materials exhibit anisotropic electronic and optical properties that are promising for applications in polarization-based optical devices [15, 16]. Black phosphorus (BP) is the first known low-symmetry 2D semiconductor layered material with a puckered honeycomb arrangement. It possesses strong in-plane optical anisotropy due to its orthorhombic crystal structure. Like other well-known 2D layered materials, it exhibits excellent properties for its potential application in optoelectronics [17]. However, there are limitations to the broader use of BP due to its poor environmental stability leading to degradation due to oxidation under ambient conditions [18]. Therefore, there is a challenge in synthesizing high-quality and large-area flakes [19]. These highlighted limitations of BP have inspired the research of alternative low-symmetry materials with environment stability such as rhenium dichalcogenides,  $\text{ReX}_2$  ( $\text{X} = \text{S, Se}$ ). Rhenium dichalcogenides fall into the class of transition metal dichalcogenides that crystallize in a distorted triclinic structure with a  $\bar{P}1$  space group [20]. This structure corresponds to a distorted  $\text{CdCl}_2$  type configuration [21, 22] caused by the Re-Re zig-zag chains formed within each layer, which breaks the in-plane symmetry. These properties lead to anisotropic optical and electronic properties, tunable bandgap, and pronounced nonlinear optical responses [23, 24], which

are ideal for applications in ultrafast photonics and high-performance photodetectors, while enabling new applications in polarization-sensitive technologies [25, 26].

Several methods have been reported for synthesis of  $\text{ReX}_2$  (X= S, Se), such as mechanical exfoliation, chemical vapor transport, liquid phase exfoliation, hydrothermal and chemical vapor deposition (CVD) [27] . Among these methods, the CVD technique has shown a precise control of material growth parameters, which is an essential feature for producing high-quality 2D materials such as rhenium diselenide ( $\text{ReSe}_2$ ) [28]. Li *et. al* reported the CVD growth high quality vertically aligned  $\text{ReSe}_2$  nanosheets directly on conductive substrates resulting in effective growth at temperatures near 450 °C [25, 29]

In this article, we report on the structural, electronic, and optical properties of high purity  $\text{ReSe}_2$  flakes synthesized by CVD technique. The morphology and elemental composition were analyzed using scanning electron microscopy (SEM), atomic force microscopy (AFM) and energy dispersive spectroscopy (EDS). The obtained images of the synthesized flakes show a triclinic crystal symmetry. The experimentally observed Raman spectra, using  $\mu$ -Raman spectroscopy, revealed 18 phonon modes that are in good agreement with the DFT calculated results. Optical absorption measurements showed distinct excitonic peaks, and X-ray diffraction (XRD) analysis confirmed the quality of the  $\text{ReSe}_2$  crystals with sharp diffraction peaks. The successful growth of  $\text{ReSe}_2$  flakes is encouraging toward the fabrication of optoelectronic devices.

## 2. Experiment

Rhenium diselenide ( $\text{ReSe}_2$ ) single crystal flakes with various thicknesses were synthesized using CVD growth method. A 100 mg of ammonium perhenate ( $\text{NH}_4\text{ReO}_4$ ) with 99.9% purity and 500 mg of selenium (Se) powdered precursors were used. These precursors were purchased from Strem Chemicals Inc. Argon and hydrogen mixed gas in a ratio of 4:1 was used as the carrier for the mass transport of thermally evaporated chemical species inside the growth

chamber. The argon-hydrogen gas mix was used as a carrier with a flow rate of 30 sccm. The growth process was conducted in a horizontal tube furnace at a temperature of 700 °C. The furnace was initially purged with Ar gas to remove any residual oxygen, ensuring an inert atmosphere. The growth time was maintained for 30 minutes to facilitate the formation of  $\text{ReSe}_2$  flakes.

A Horiba LabRAM HR spectrometer was used to obtain  $\mu$ -photoluminescence (PL) and  $\mu$ -Raman spectra. A HeNe laser of a wavelength of 632.8 nm was used to investigate Raman vibrational modes. The spectra range of the data collected is between  $100 - 300 \text{ cm}^{-1}$ . A Cobalt laser of a wavelength of 472.9 nm was used for the PL measurement spanning spectral range of 450 – 1100 nm. Angle-resolved polarized Raman spectroscopy was carried out to determine the in-plane anisotropy and crystallographic orientation of the sample. Polarization rotation was performed by rotating a half-wave plate through rotation angle varied from  $0^\circ$  to  $360^\circ$  in  $10^\circ$  increments. At each angle, Raman spectra were acquired under identical integration conditions and processed to extract peak intensities. The absorbance spectrum was obtained using Cary 500 UV-Visible-NIR by Agilent. Structural analysis of the synthesized  $\text{ReSe}_2$  was conducted using an X-ray diffractometer (Rigaku Miniflex) equipped with Cu  $\text{K}\alpha$  radiation ( $\lambda = 1.5406 \text{ \AA}$ ). The diffraction patterns collected were over a  $2\theta$  range of  $10 - 60^\circ$  to identify the crystalline phases and assess the quality of the deposited layers. A Bruker D3100 Nanoscope AFM, equipped with a tapping mode module, was utilized to investigate the surface morphology of the grown  $\text{ReSe}_2$  flakes. The SEM images were obtained by using a FEI Nova Nanolab 200 fitted with a Bruker EDS detector.

### 3. Theory

Theoretical investigations were performed using DFT computational method as implemented in Vienna *ab initio* simulation package (VASP) [30, 31]. The generalized gradient

approximation (GGA) with the Perdew–Burke–Ernzerhof (PBE) is adopted for the exchange–correlation functionals [32]. The Van der Waals interactions were considered in these calculations using the optB86b functional [33]. A plane-wave cutoff energy of 550 eV was employed with energy convergence criterion set at  $10^{-8}$  eV. The Brillouin zone was sampled using  $9 \times 9 \times 8$  and  $9 \times 9 \times 1$  Monkhorst–Pack K -point grids for the bulk and monolayer systems, respectively. The density functional perturbation theory (DFPT) technique [34] was used to obtain the phonon modes at the gamma point. The layered stacking of  $\text{ReSe}_2$  structure is composed of rhenium atoms sandwiched between the selenium atoms as shown in Fig. 1 (a) and (b). This figure shows the distorted triclinic structure known as Peierls distortion, where the Re atoms form Re-Re chains with diamond shape.

#### 4. Results and Discussion

The AFM details of  $\text{ReSe}_2$  flakes grown on  $\text{SiO}_2/\text{Si}$  substrate with the height distribution is represented by Fig. 2(a) in a range of values from 5-50 nm indicated by the profile height scan. The surface topography as presented in Fig (2b) reveals the flakes morphology with varying thickness across the scanned area. The line profile corresponds to the thickness as depicted by the color markers green, blue, and red have the values 50, 10, and 5 nm, respectively. It is observed that the bright island spots are thicker in dimensions than the dim ones. Therefore, the variation in height is suggestive of multilayered  $\text{ReSe}_2$  formation ranging from few to several layers in agreement with Hafeez, *et al.* [35].

The surface morphology of  $\text{ReSe}_2$  flakes is obtained by SEM, which shows well-defined hexagonal-like structure with varying thickness as indicated in Fig. 3. The presence of layered structures as seen from the SEM image is typical for van der Waals 2D layered materials along the

basal plane direction [36]. The stoichiometry of the atomic percentage of Re:Se is 1:2 as confirmed by the EDS as reported in Table I.

The X-ray diffraction (XRD) spectrum as shown in Fig. 4 has well defined peaks at diffraction angles  $14.4^\circ$ ,  $28.5^\circ$ ,  $42.9^\circ$  and  $58.2^\circ$ , which are readily indexed as (002), (004), (0 0 6), and (0 0 8) crystal planes of the layered  $\text{ReSe}_2$ , respectively. These observed peaks positions are characteristics of crystalline, layered  $\text{ReSe}_2$  with distorted triclinic crystal symmetry, which matches the ICDD card No. 04-007-1113 [24, 37]. We note the observation of no other noticeable peaks except the well resolved XRD patterns of  $\text{ReSe}_2$ , emphasizing the quality of the growth.

The  $\mu$ -Raman spectra of the grown  $\text{ReSe}_2$  were taken at room temperature as shown in Fig. 5. This spectrum revealed the presence of the expected and well-defined 18 Raman modes. The experimentally observed Raman modes are consistent with the computational values using the DFPT method [22, 25] as shown in Table II. These observed Raman modes mostly possess  $A_g$  symmetry which corresponds to the in-plane vibrational modes [38, 39]. The active Raman modes of vibrations within the short range ( $100 - 300 \text{ cm}^{-1}$ ) further indicate the low symmetry properties of  $\text{ReSe}_2$  with an anisotropic behavior due to its triclinic crystal symmetry. This anisotropic behavior distinguishes its optical and electronics responses [39] from other transition-metal dichalcogenides (TMDs) with high symmetry such as  $\text{WS}_2$  and  $\text{MoS}_2$ .

The polarization polar plot of three selected Raman modes ( $125.3$ ,  $162$ , and  $177 \text{ cm}^{-1}$ ) from the experimental data were analyzed to understand the optical anisotropy of the grown  $\text{ReSe}_2$ . The resulting polar plot takes the form of a two-lobe shape characteristics of anisotropic low-symmetric 2D materials [40]. However, the lobes display unequal intensity maxima, indicating a deviation from ideal symmetric anisotropic scattering. This can be attributed to the surface roughness, morphology [41] and thickness variation [42] from the growth process as evidenced by the SEM

image in Fig. 3. This premise resulted in altering the incident polarization and the scattered intensities thereby modifying the effective Raman tensor. To account for the asymmetric behavior and describe the angular dependence of the Raman signal, the scattering intensity is expressed through the Raman tensor ( $R$ ) and the unit polarization vectors of the incident ( $e_i$ ) and scattered ( $e_s$ ) light [43].

$$I \propto |e_i R e_s|^2 \quad (1)$$

Equation (2) was used to fit the polar plot where  $\theta$  is polarization incident angle made with crystal which is oriented along the distorted Re-Re chain where the maximum intensities are observed

$$I(\theta) \propto v^2 + u^2 \cos^2 \theta + w^2 \sin^2 \theta + 2v(u + w) \cos \theta \sin \theta \quad (2) [22]$$

where  $u$ ,  $v$ , and  $w$  are the elements for each vibrational mode given by  $2 \times 2$  matrix  $R = \begin{pmatrix} u & v \\ v & w \end{pmatrix}$  and the polarization angle,  $\theta$ , is obtained from the  $\tan 2\theta = \frac{2v}{u-w}$ . From the polarization-dependent Raman analysis, the angular dependence of the selected Raman modes (125.3, 162.3, and 177  $\text{cm}^{-1}$ ) was fitted using equation (2). The results are shown in Fig. 6 where the black squares represent the measured angle-resolved Raman intensities, and the solid red curves correspond to the tensor-based fitted profiles. The vibrational modes at 125.3 and 162.3  $\text{cm}^{-1}$  exhibit their maximum intensities near  $80^\circ$  and  $260^\circ$ , whereas the 177  $\text{cm}^{-1}$  mode displays a slightly shifted pair of maxima at approximately  $75^\circ$  and  $255^\circ$ . The observed  $180^\circ$  periodicity in the different modes is characteristic of the two-fold angular symmetry expected for strongly anisotropic 2D materials [44, 45]. The variation in the polarization angles of maximum intensity among the different modes indicates mode-dependent Raman tensor orientations and reflects the underlying preferential alignment of the distorted Re-Re atomic chains. The results of the fitting tensor parameters and the extracted polarization directions for each mode are summarized in Table III.

The non-zero and non-equivalent values of the tensor fitted parameters ensure the angular dependency for each vibrational modes, this outcome confirms the anisotropic nature of ReSe<sub>2</sub>.

The room-temperature absorption measurement of the grown ReSe<sub>2</sub> is presented in Fig. 7. The absorption spectra exhibit two prominent excitonic peaks located at 942 nm (red line) and 885 nm (blue line), corresponding to energy transition with approximate values of 1.32 eV and 1.40 eV, respectively. These excitonic features indicate a slight layer-dependent variation in the optical bandgap. The obtained bandgap values are consistent with the results reported by Huang *et al.*, who observed temperature-dependent excitonic transitions ranging from 1.36 to 1.42 eV in polarization-resolved absorption measurements between 25 K and 525 K [46, 47]. The close agreement between our room-temperature measurements and their temperature-dependent study further validates that excitonic transitions exist regardless of temperature variation. The slight blue shift of the higher-energy peak to 1.40 eV in our measurement can be attributed to the reduced layer thickness in the grown flakes. The bandgap showed slight variation with thickness, suggesting that there is a weak degree of quantum confinement at the nanoscale [23, 48, 49]. However, it is not pronounced when compared to other traditional TMDs, such as MoS<sub>2</sub>, WS<sub>2</sub>, or ReS<sub>2</sub> where studies have demonstrated a strong quantum confinement effect [45, 50, 51].

The electronic band structure combined with the partial density of states for both bulk and monolayer ReSe<sub>2</sub>, obtained using DFT calculations, are represented by Fig. 8(a, b). The energy bandgap of the bulk is found to be indirect, having an energy value of 0.88 eV [20, 22] with the maximum of the valence band located at the  $\Gamma$  points, while its conduction band minimum is located between R and  $\Gamma$  points. However, the monolayer band structure shows a direct bandgap of 1.26 eV at the  $\Gamma$  high symmetry point [52]. Equally, the partial density of states calculation showed the orbitals contribution of each element, which perfectly describe the electronic properties

in both the bulk and monolayer form. The conduction band is dominated by the d-orbital of the Re atoms while the valence band has almost equal contribution of both the d-orbit of Re and p-orbit of Se atoms. The DFT predicted bandgaps showed slight observable increase in bandgaps. This further established the weak interlayer dependence of the bandgap as reported in other DFT based studies for  $\text{ReSe}_2$  [53].

The room temperature PL measurement as represented by the black line in Fig. 9 exhibits a broad spectrum of optical transitions with one main peak around 770 nm (1.60 eV) and two shoulders at 670 nm (1.85 eV) and 860 nm (1.44 eV). This spectrum is fitted with a Gaussian line shape (see a magenta line) to indicate the presence of three main peaks. Gaussian curves (green, blue, and red) were added to resolve the presence of the three peaks. These three peaks represent excitonic transitions within the flake under the assumption that the electrons were not undergoing transitions from the valence band to different minima in the conduction band. The transitions are rather generated from the same flake with nonuniform thickness such that the quantum confinement is not uniform within the flake. The three excitonic transitions correspond to the band gap values. The experimentally reported results of the band gaps are found to be higher than those predicted by DFT calculations as shown in Fig. 7. This can be attributed to the approximation method associated with DFT, which leads to bandgap underestimation. However, the observed high energy excitonic value of 1.85 eV (green curve) from Fig. 9 is consistent with the first-principles GW-Bethe-Salpeter equation approach prediction in the study of  $\text{ReSe}_2$  by Zhong *et al.* [54], which is around 2.09 eV for suspended monolayer  $\text{ReSe}_2$ . The latter band gap value is higher than the experimental results due to depressed screening and reduced dimension thereby enhancing quantum confinement [17, 55-57].

## 5. Conclusion

Highly crystalline anisotropic layered  $\text{ReSe}_2$  flakes with hexagonal structures were successfully grown via CVD. The Raman scattering spectrum reveals the presence of 18 phonon modes in the range of  $100 - 300 \text{ cm}^{-1}$ , which agrees with the computational predictions, indicating accurate phonon dispersion in the material. Density Functional Theory (DFT) calculations predicted an indirect bandgap of  $0.88\text{eV}$  for the bulk and  $1.26\text{eV}$  for the monolayer of  $\text{ReSe}_2$ . The absorption spectra of the grown  $\text{ReSe}_2$  were found to be in the near-infrared region, between  $885 - 942 \text{ nm}$ , suggesting layer-dependent optical response. The energy bandgap values obtained from photoluminescence measurement further confirm the layer dependent nature of  $\text{ReSe}_2$  with an optical energy emission between  $1.44 - 1.85 \text{ eV}$ , this implies its application ranges from visible to near infrared region-based optoelectronics devices. Scanning electron microscopy and energy-dispersive X-ray spectroscopy confirm the quality and morphology of the material with the profile height between  $5-50 \text{ nm}$  measured by AFM.

## Credit authorship contribution statement

Juwon Onasanya (J.O.): Writing – original draft, Software, Methodology, Investigation, Data curation. Mourad Benamara: Validation, Resources, Formal analysis, Data curation. Kanagaraj Moorthi: Validation, Resources, Formal analysis, Data curation. Bothina Hamad (B.H.): Validation, Supervision, Software, Methodology, Funding acquisition, Conceptualization. H. O. H. Churchill: Validation, Project administration, Funding acquisition, Conceptualization. M.O. Manasreh: Validation, Supervision, Project administration, Funding acquisition, Conceptualization

## **Declaration of Competing Interest**

The authors declare that they have no known competing financial interests or personal relationships that could have appeared to influence the work reported in this paper.

## **Acknowledgment**

**B.H.** thanks the support of the MonArk Quantum Foundry that is funded by the National Science Foundation Q-AMASE-i program under NSF Award No. DMR-1906383. In addition, **B.H.** declares that this material is based upon work supported by the National Science Foundation under Award No. DGE-2244274. DMR-1906383. **J.O.** declares that this material is based on research sponsored by AFRL under agreement number FA8750-24-1-1019. The U.S. Government is authorized to reproduce and distribute reprints for Governmental purposes notwithstanding any copyright notation thereon. The authors would like to thank Arkansas High Performance Computing Center (AHPCC), University of Arkansas, for the computing resources.

## **Data availability**

Data will be made available on reasonable request.

## **References**

- [1] A. She, Y. Zhao, J. Ni and Z. Dai, "The influence of lattice anharmonicity on the thermal transport properties of two-dimensional MgF<sub>2</sub>," Journal of Physics D: Applied Physics, vol. 58, p. 045305, November 2024. <https://doi.org/10.1088/1361-6463/ad8d4e>

[2] J. Fang, Z. Zhou, M. Xiao, Z. Lou, Z. Wei and G. Shen, "Recent advances in low-dimensional semiconductor nanomaterials and their applications in high-performance photodetectors," *InfoMat*, vol. 2, p. 291–317, December 2019. <https://doi.org/10.1002/inf2.12067>

[3] K. S. Thygesen, "Calculating excitons, plasmons, and quasiparticles in 2D materials and van der Waals heterostructures," *2D Materials*, vol. 4, p. 022004, June 2017. <https://doi.org/10.1088/2053-1583/aa6432>

[4] L. Du, T. Hasan, A. Castellanos-Gomez, G.-B. Liu, Y. Yao, C. N. Lau and Z. Sun, "Engineering symmetry breaking in 2D layered materials," *Nature Reviews Physics*, vol. 3, p. 193–206, February 2021. <https://doi.org/10.1038/s42254-020-00276-0>

[5] F. B. Sousa, R. Nadas, R. Martins, A. P. M. Barboza, J. S. Soares, B. R. A. Neves, I. Silvestre, A. Jorio and L. M. Malard, "Disentangling doping and strain effects at defects of grown MoS<sub>2</sub> monolayers with nano-optical spectroscopy," *Nanoscale*, vol. 16, p. 12923–12933, 2024. <https://doi.org/10.1039/d4nr00837e>

[6] S. Wang, N. T. Hung and M. Sun, "Two-Dimensional Materials: From Synthesis to Applications," *Molecules*, vol. 30, p. 741, February 2025. <https://doi.org/10.3390/molecules30030741>

[7] W. Xu, P. Guo, X. Li, Z. Hui, Y. Wang, Z. Shi and Y. Shu, "Sheet-structured bismuthene for near-infrared dual-wavelength harmonic mode-locking," *Nanotechnology*, vol. 31, p. 225209, March 2020. <https://doi.org/10.1088/1361-6528/ab7674>

[8] S.-Y. Yue, T. Xu and B. Liao, "Ultralow thermal conductivity in a two-dimensional material due to surface-enhanced resonant bonding," *Materials Today Physics*, vol. 7, p. 89–95, December 2018. <https://doi.org/10.1016/j.mtphys.2018.11.005>

[9] N. Peimyoo, H.-Y. Wu, J. Escolar, A. De Sanctis, G. Prando, F. Vollmer, F. Withers, A. C. Riis-Jensen, M. F. Craciun, K. S. Thygesen and S. Russo, "Engineering Dielectric Screening for Potential-well Arrays of Excitons in 2D Materials," *ACS Applied Materials & Interfaces*, vol. 12, p. 55134–55140, November 2020. <https://doi.org/10.1021/acsami.0c14696>

[10] D. B. Straus and C. R. Kagan, "Electrons, Excitons, and Phonons in Two-Dimensional Hybrid Perovskites: Connecting Structural, Optical, and Electronic Properties," *The Journal of Physical Chemistry Letters*, vol. 9, p. 1434–1447, February 2018. <https://doi.org/10.1021/acs.jpclett.8b00201>

[11] X. Wang, T. Garcia, S. Monaco, B. Schatschneider and N. Marom, "Effect of crystal packing on the excitonic properties of rubrene polymorphs," *CrystEngComm*, vol. 18, p. 7353–7362, 2016. <https://doi.org/10.1039/c6ce00873a>

[12] Y. Yang, S.-C. Liu, W. Yang, Z. Li, Y. Wang, X. Wang, S. Zhang, Y. Zhang, M. Long, G. Zhang, D.-J. Xue, J.-S. Hu and L.-J. Wan, "Air-Stable In-Plane Anisotropic GeSe<sub>2</sub> for Highly Polarization-Sensitive Photodetection in Short Wave Region," *Journal of the*

American Chemical Society, vol. 140, p. 4150–4156, March 2018.  
<https://doi.org/10.1021/jacs.8b01234>

- [13] X. Ling, H. Wang, S. Huang, F. Xia and M. S. Dresselhaus, "The renaissance of black phosphorus," *Proceedings of the National Academy of Sciences*, vol. 112, p. 4523–4530, March 2015. <https://doi.org/10.1073/pnas.1416581112>
- [14] S. Puebla, R. D'Agosta, G. Sanchez-Santolino, R. Frisenda, C. Munuera and A. Castellanos-Gomez, "In-plane anisotropic optical and mechanical properties of two-dimensional MoO<sub>3</sub>," *npj 2D Materials and Applications*, vol. 5, April 2021. <https://doi.org/10.1038/s41699-021-00220-5>
- [15] B. Aslan, D. A. Chenet, A. M. van der Zande, J. C. Hone and T. F. Heinz, "Linearly Polarized Excitons in Single- and Few-Layer ReS<sub>2</sub> Crystals," *ACS Photonics*, vol. 3, p. 96–101, December 2015. <https://doi.org/10.1021/acspophotonics.5b00486>
- [16] Y. Xiong, H. Chen, D. W. Zhang and P. Zhou, "Electronic and Optoelectronic Applications Based on ReS<sub>2</sub>," *physica status solidi (RRL) – Rapid Research Letters*, vol. 13, February 2019. <https://doi.org/10.1002/pssr.201800658>
- [17] V. Tran, R. Soklaski, Y. Liang and L. Yang, "Layer-controlled band gap and anisotropic excitons in few-layer black phosphorus," *Physical Review B*, vol. 89, p. 235319, June 2014. <https://doi.org/10.1103/physrevb.89.235319>
- [18] W. Dickerson, V. Tayari, I. Fakih, A. Korinek, M. Caporali, M. Serrano-Ruiz, M. Peruzzini, S. Heun, G. A. Botton and T. Szkopek, "Phosphorus oxide gate dielectric for black phosphorus field effect transistors," *Applied Physics Letters*, vol. 112, April 2018. <https://doi.org/10.1063/1.5011424>
- [19] N. Wang, N. Mao, Z. Wang, X. Yang, X. Zhou, H. Liu, S. Qiao, X. Lei, J. Wang, H. Xu, X. Ling, Q. Zhang, Q. Feng and J. Kong, "Electrochemical Delamination of Ultralarge Few-Layer Black Phosphorus with a Hydrogen-Free Intercalation Mechanism," *Advanced Materials*, vol. 33, November 2020. <https://doi.org/10.1002/adma.202005815>
- [20] D. A. Chenet, B. Aslan, P. Y. Huang, C. Fan, A. M. van der Zande, T. F. Heinz and J. C. Hone, "In-Plane Anisotropy in Mono- and Few-Layer ReS<sub>2</sub> Probed by Raman Spectroscopy and Scanning Transmission Electron Microscopy," *Nano Letters*, vol. 15, p. 5667–5672, August 2015. <https://doi.org/10.1021/acs.nanolett.5b00910>
- [21] H.-J. Lamfers, A. Meetsma, G. A. Wiegers and J. L. de Boer, "The crystal structure of some rhenium and technetium dichalcogenides," *Journal of Alloys and Compounds*, vol. 241, p. 34–39, August 1996. [https://doi.org/10.1016/0925-8388\(96\)02313-4](https://doi.org/10.1016/0925-8388(96)02313-4)
- [22] D. Wolverton, S. Crampin, A. S. Kazemi, A. Ilie and S. J. Bending, "Raman Spectra of Monolayer, Few-Layer, and Bulk ReSe<sub>2</sub>: An Anisotropic Layered Semiconductor," *ACS Nano*, vol. 8, p. 11154–11164, November 2014. <https://doi.org/10.1021/nn5053926>

[23] K. Kadiwala, L. Dipane, E. Dipans, A. Bundulis, M. Zubkins, A. Ogurcovs, J. Gabrusenoks, D. Bocharov, E. Butanovs and B. Polyakov, "Synthesis and Investigation of ReSe<sub>2</sub> Thin Films Obtained from Magnetron Sputtered Re and ReO<sub>x</sub>," *Crystals*, vol. 14, p. 690, July 2024. <https://doi.org/10.3390/cryst14080690>

[24] S. Yang, S. Tongay, Y. Li, Q. Yue, J.-B. Xia, S.-S. Li, J. Li and S.-H. Wei, "Layer-dependent electrical and optoelectronic responses of ReSe<sub>2</sub> nanosheet transistors," *Nanoscale*, vol. 6, p. 7226, 2014. <https://doi.org/10.1039/c4nr01741b>

[25] Y. Rho, J. Pei, L. Wang, Z. Su, M. Eliceiri and C. P. Grigoropoulos, "Site-Selective Atomic Layer Precision Thinning of MoS<sub>2</sub> via Laser-Assisted Anisotropic Chemical Etching," *ACS Applied Materials & Interfaces*, vol. 11, p. 39385–39393, September 2019. <https://doi.org/10.1021/acsami.9b14306>

[26] L. Loh, Z. Zhang, M. Bosman and G. Eda, "Substitutional doping in 2D transition metal dichalcogenides," *Nano Research*, vol. 14, p. 1668–1681, August 2020. <https://doi.org/10.1007/s12274-020-3013-4>

[27] J. Peng, Z.-j. Chen, B. Ding and H.-M. Cheng, "Recent Advances for the Synthesis and Applications of 2-Dimensional Ternary Layered Materials," *Research*, vol. 6, January 2023. <https://doi.org/10.34133/research.0040>

[28] Y. Zhang, Y. Yao, M. G. Sendeku, L. Yin, X. Zhan, F. Wang, Z. Wang and J. He, "Recent Progress in CVD Growth of 2D Transition Metal Dichalcogenides and Related Heterostructures," *Advanced Materials*, vol. 31, August 2019. <https://doi.org/10.1002/adma.201901694>

[29] J. Li, Q. Zhou, C. Yuan, P. Cheng, X. Hu, W. Huang, X. Gao, X. Wang, M. Jin, R. Nötzel, G. Zhou, Z. Zhang and J. Liu, "Direct growth of vertically aligned ReSe<sub>2</sub> nanosheets on conductive electrode for electro-catalytic hydrogen production," *Journal of Colloid and Interface Science*, vol. 553, p. 699–704, October 2019. <https://doi.org/10.1016/j.jcis.2019.06.073>

[30] G. Kresse and J. Hafner, "Ab initio molecular dynamics for liquid metals," *Physical Review B*, vol. 47, p. 558–561, January 1993. <https://doi.org/10.1103/physrevb.47.558>

[31] G. Kresse and J. Furthmüller, "Efficient iterative schemes for ab initio total-energy calculations using a plane-wave basis set," *Physical Review B*, vol. 54, p. 11169–11186, October 1996. <https://doi.org/10.1103/physrevb.54.11169>

[32] J. P. Perdew, K. Burke and M. Ernzerhof, "Generalized Gradient Approximation Made Simple," *Physical Review Letters*, vol. 77, p. 3865–3868, October 1996. <https://doi.org/10.1103/physrevlett.77.3865>

[33] J. Klimeš, D. R. Bowler and A. Michaelides, "Van der Waals density functionals applied to solids," *Physical Review B*, vol. 83, p. 195131, May 2011. <https://doi.org/10.1103/physrevb.83.195131>

[34] S. Baroni, S. de Gironcoli, A. Dal Corso and P. Giannozzi, "Phonons and related crystal properties from density-functional perturbation theory," *Reviews of Modern Physics*, vol. 73, p. 515–562, July 2001. <https://doi.org/10.1103/revmodphys.73.515>

[35] M. Hafeez, L. Gan, H. Li, Y. Ma and T. Zhai, "Chemical Vapor Deposition Synthesis of Ultrathin Hexagonal ReSe<sub>2</sub> Flakes for Anisotropic Raman Property and Optoelectronic Application," *Advanced Materials*, vol. 28, p. 8296–8301, July 2016. <https://doi.org/10.1002/adma.201601977>

[36] P. Sutter and E. Sutter, "Unconventional van der Waals heterostructures beyond stacking," *iScience*, vol. 24, p. 103050, September 2021. <https://doi.org/10.1016/j.isci.2021.103050>

[37] B. Jariwala, D. Voiry, A. Jindal, B. A. Chalke, R. Bapat, A. Thamizhavel, M. Chhowalla, M. Deshmukh and A. Bhattacharya, "Synthesis and Characterization of ReS<sub>2</sub> and ReSe<sub>2</sub> Layered Chalcogenide Single Crystals," *Chemistry of Materials*, vol. 28, p. 3352–3359, May 2016. <https://doi.org/10.1021/acs.chemmater.6b00364>

[38] V. O. Yukhymchuk, L. M. Kulikov, M. Y. Valakh, A. P. Litvinchuk, M. A. Skoryk, N. V. Mazur, V. S. Yefanov, O. Selyshchev, V. M. Dzhagan and D. R. T. Zahn, "Structure and vibrational spectra of ReSe<sub>2</sub> nanoplates," *Journal of Raman Spectroscopy*, vol. 51, p. 1305–1314, May 2020. <https://doi.org/10.1002/jrs.5898>

[39] E. Lorchat, G. Froehlicher and S. Berciaud, "Splitting of Interlayer Shear Modes and Photon Energy Dependent Anisotropic Raman Response in N-Layer ReSe<sub>2</sub> and ReS<sub>2</sub>," *ACS Nano*, vol. 10, p. 2752–2760, February 2016. <https://doi.org/10.1021/acsnano.5b07844>

[40] K. Friemelt, M.-C. Lux-Steiner and E. Bucher, "Optical properties of the layered transition-metal-dichalcogenide ReS<sub>2</sub>: Anisotropy in the van der Waals plane," *Journal of Applied Physics*, vol. 74, p. 5266–5268, October 1993. <https://doi.org/10.1063/1.354268>

[41] S. Y. Park, H. Rho, J. D. Song, S. Lee, G. Kim and C. H. Lee, "Spatially-resolved and polarized Raman scattering from a single Si nanowire," *Journal of Raman Spectroscopy*, vol. 46, p. 524–530, April 2015. <https://doi.org/10.1002/jrs.4689>

[42] R. P. N. Tripathi, X. Yang and J. Gao, "Polarization-dependent optical responses in natural 2D layered mineral teallite," *Scientific Reports*, vol. 11, November 2021. <https://doi.org/10.1038/s41598-021-01511-z>

[43] Z. Shu, Q. Peng, P. Huang, Z. Xu, A. A. Suleiman, X. Zhang, X. Bai, X. Zhou and T. Zhai, "Growth of Ultrathin Ternary Teallite (PbSnS<sub>2</sub>) Flakes for Highly Anisotropic Optoelectronics," *Matter*, vol. 2, p. 977–987, April 2020. <https://doi.org/10.1016/j.matt.2020.01.013>

[44] G. Nam, S. Park, K. Heo, J. Bong, D. Lee, H. Kim, K. M. Ponnusamy, H. Bae, H. G. Park, J.-H. Lee and H.-S. Jang, "An in-depth study of the synthesis of ReSe<sub>2</sub> for anisotropic

Raman characteristics," *Journal of Physics: Materials*, vol. 7, p. 045005, October 2024. <https://doi.org/10.1088/2515-7639/ad8033>

- [45] F. Cui, X. Li, Q. Feng, J. Yin, L. Zhou, D. Liu, K. Liu, X. He, X. Liang, S. Liu, Z. Lei, Z. Liu, H. Peng, J. Zhang, J. Kong and H. Xu, "Epitaxial growth of large-area and highly crystalline anisotropic ReSe<sub>2</sub> atomic layer," *Nano Research*, vol. 10, p. 2732–2742, April 2017. <https://doi.org/10.1007/s12274-017-1477-7>
- [46] Y.-C. Jian, D.-Y. Lin, J.-S. Wu and Y.-S. Huang, "Optical and Electrical Properties of Au- and Ag-Doped ReSe<sub>2</sub>," *Japanese Journal of Applied Physics*, vol. 52, p. 04CH06, February 2013. <https://doi.org/10.7567/jjap.52.04ch06>
- [47] Y. S. Huang, C. H. Ho, P. C. Liao and K. K. Tiong, "Temperature dependent study of the band edge excitons of ReS<sub>2</sub> and ReSe<sub>2</sub>," *Journal of Alloys and Compounds*, vol. 262–263, p. 92–96, November 1997. [https://doi.org/10.1016/s0925-8388\(97\)00335-6](https://doi.org/10.1016/s0925-8388(97)00335-6)
- [48] R. Dutta, A. Bala, A. Sen, M. R. Spinazze, H. Park, W. Choi, Y. Yoon and S. Kim, "Optical Enhancement of Indirect Bandgap 2D Transition Metal Dichalcogenides for Multi-Functional Optoelectronic Sensors," *Advanced Materials*, vol. 35, September 2023. <https://doi.org/10.1002/adma.202303272>
- [49] H. Zhao, J. Wu, H. Zhong, Q. Guo, X. Wang, F. Xia, L. Yang, P. Tan and H. Wang, "Interlayer interactions in anisotropic atomically thin rhenium diselenide," *Nano Research*, vol. 8, p. 3651–3661, October 2015. <https://doi.org/10.1007/s12274-015-0865-0>
- [50] E. Zhang, P. Wang, Z. Li, H. Wang, C. Song, C. Huang, Z.-G. Chen, L. Yang, K. Zhang, S. Lu, W. Wang, S. Liu, H. Fang, X. Zhou, H. Yan, J. Zou, X. Wan, P. Zhou, W. Hu and F. Xiu, "Tunable Ambipolar Polarization-Sensitive Photodetectors Based on High-Anisotropy ReSe<sub>2</sub> Nanosheets," *ACS Nano*, vol. 10, p. 8067–8077, August 2016. <https://doi.org/10.1021/acsnano.6b04165>
- [51] S. Ojo, J. Onasanya, M. Benamara, B. Hamad and M. O. Manasreh, "Optical spectroscopy of excitons in ReS<sub>2</sub> monolayers grown by chemical vapor deposition," *Optical Materials*, vol. 160, p. 116729, March 2025. <https://doi.org/10.1016/j.optmat.2025.116729>
- [52] J.-Q. Zong, W.-X. Ji, P. Li and P.-J. Wang, "The biaxial strain induced properties of ReX<sub>2</sub> and ReXS (X = S, Se, Te) monolayers," *Materials Research Express*, vol. 7, p. 055018, May 2020. <https://doi.org/10.1088/2053-1591/ab7218>
- [53] A. Arora, J. Noky, M. Drüppel, B. Jariwala, T. Deilmann, R. Schneider, R. Schmidt, O. Del Pozo-Zamudio, T. Stiehm, A. Bhattacharya, P. Krüger, S. Michaelis de Vasconcellos, M. Rohlfing and R. Bratschitsch, "Highly Anisotropic in-Plane Excitons in Atomically Thin and Bulklike 1T'-ReSe<sub>2</sub>," *Nano Letters*, vol. 17, p. 3202–3207, April 2017. <https://doi.org/10.1021/acs.nanolett.7b00765>
- [54] H.-X. Zhong, S. Gao, J.-J. Shi and L. Yang, "Quasiparticle band gaps, excitonic effects, and anisotropic optical properties of the monolayer distorted 1T-diamond-chain structures

ReS<sub>2</sub> and ReSe<sub>2</sub>" Physical Review B, vol. 92, p. 115438, September 2015. <https://doi.org/10.1103/physrevb.92.115438>

[55] D. Y. Qiu, F. H. da Jornada and S. G. Louie, "Optical Spectrum of MoS<sub>2</sub>: Many-Body Effects and Diversity of Exciton StatesMany-Body Effects and Diversity of Exciton States," Physical Review Letters, vol. 111, p. 216805, November 2013. <https://doi.org/10.1103/physrevlett.111.216805>

[56] C. D. Spataru, S. Ismail-Beigi, L. X. Benedict and S. G. Louie, "Excitonic Effects and Optical Spectra of Single-Walled Carbon Nanotubes," Physical Review Letters, vol. 92, p. 077402, February 2004. <https://doi.org/10.1103/physrevlett.92.077402>

[57] A. Ramasubramaniam, "Large excitonic effects in monolayers of molybdenum and tungsten dichalcogenides," Physical Review B, vol. 86, p. 115409, September 2012. <https://doi.org/10.1103/physrevb.86.115409>

### Figure Caption

Fig. 1(a) Top view showing the zig-zig arrangement of rhenium atoms in ReSe<sub>2</sub> structure (b) Side view ReSe<sub>2</sub> structure with the Rhenium atoms sandwiched between the selenium atoms.

Fig. 2 (a) Height profile measurement of scanned flakes, the colors correspond to each identified spot on the AFM image. (b) AFM image showing the grown ReSe<sub>2</sub> flakes.

Fig. 3 SEM image of ReSe<sub>2</sub> flakes with hexagonal-like layered structure.

Fig. 4 X-ray diffraction pattern of ReSe<sub>2</sub> flakes with its characteristic peaks indexed at (002), (004), (006), and (008) showing preferential orientations along the c-axis typical for 2D layered ReSe<sub>2</sub>.

Fig. 5 The micro-Raman spectrum of ReSe<sub>2</sub> at room temperature with 18 observable phonon modes in the range of 100 – 300 cm<sup>-1</sup>. The observed vibrational modes are consistent for a typical triclinic ReSe<sub>2</sub> and are in good agreement with DFT calculations.

Fig. 6 Angle-resolved polarized Raman polar plot of the intensity of the vibrational mode at (a) 125.3 (b) 162.3 cm<sup>-1</sup> and (c) 176.1 cm<sup>-1</sup> as a function of the polarization angle. Black squares indicate experimental data points, and the solid red line represents the theoretical fit derived from the Raman tensor analysis. (d) Optical microscope image of the scanned ReSe<sub>2</sub> flake for polarization measurements.

Fig. 7 The room temperature absorbance spectra plot of ReSe<sub>2</sub> flakes with observed maximum wavelength peaks at 885 and 942 nm.

Fig. 8 (a) The density functional theory calculation of combined plot of density of states and energy bandgap for bulk ReSe<sub>2</sub> with energy value of 0.88 eV. (b) The density functional theory calculation of combined plot of density of states and energy bandgap for monolayer ReSe<sub>2</sub> with energy value of 1.26 eV.

Fig. 9 The guassian fit of room temperature PL measurement of CVD grown ReSe<sub>2</sub> flake. The color black represent the experimental curve while the other colors green, blue, and red are

the corresponding guassian curves for the excitonic peaks. The peaks value for the fitted curve are 670 nm (1.85 eV), 770 nm (1.61 eV) and 860 nm (1.44 eV).

Table I. Energy-dispersive spectroscopy elemental composition of  $\text{ReSe}_2$  flakes.

Elements	Series	Concentration (Atomic Weight %)	Error
Re	L- series	24.59	1.63
Se	L- series	45.07	1.76

Table II. Raman modes for experimentally measured and DFT calculated for  $\text{ReSe}_2$  both in the range of  $100 - 300 \text{ cm}^{-1}$  with a total of 18 raman active peaks.

Peak Numbers	Experiment ( $\text{cm}^{-1}$ )	Calculated ( $\text{cm}^{-1}$ )	Raman Mode
1	116.3	112.7	$\text{A}_g$
2	122.1	117.9	$\text{A}_g$
3	125.3	122.8	$\text{A}_g$
4	128.5	125.5	$\text{A}_g$
5	162.3	159.4	$\text{A}_g$
6	176.1	172.0	$\text{A}_g$
7	180.7	177.1	$\text{A}_g$
8	184.2	179.9	$\text{A}_g$
9	195.3	192.0	$\text{A}_g$
10	200.0	195.1	$\text{A}_g$
11	213.6	208.2	$\text{A}_g$
12	221.5	219.7	$\text{A}_g$
13	236.4	236.6	$\text{A}_g$
14	243.5	241.3	$\text{A}_g$
15	251.1	249.8	$\text{A}_g$
16	264.5	262.3	$\text{A}_g$
17	287.5	285.1	$\text{A}_g$
18	297.3	295.3	$\text{A}_g$

Table III. Angle-resolved polarized Raman-tensor fit ( $u$ ,  $v$ ,  $w$ ) and polarization angle ( $\theta$ )

Peak (cm <sup>-1</sup> )	u	v	w	$\theta_{max}$	$\theta_{max} + 180^\circ$
125.3	2.40	13.02	70.95	80°	260°
162.1	9.39497	5.1785	32.25	77.8°	257.8°
176.3	15.000	10.53908	49.99	74.5°	254.5

Table IV. Summary of the energy bandgap for PL gaussian fits, DFT-calculated bandgap, and experimental absorption for  $\text{ReSe}_2$ .

	PL (eV)	Absorption (Expt.) (eV)	DFT-Bandgap (eV)
$\text{ReSe}_2$ (Bulk)			0.88
$\text{ReSe}_2$ (Monolayer)			1.26
Thick flakes		1.32	
Thin flakes		1.40	
Fit peak 3	1.44		
Fit peak 2	1.60		
Fit peak 1	1.85		

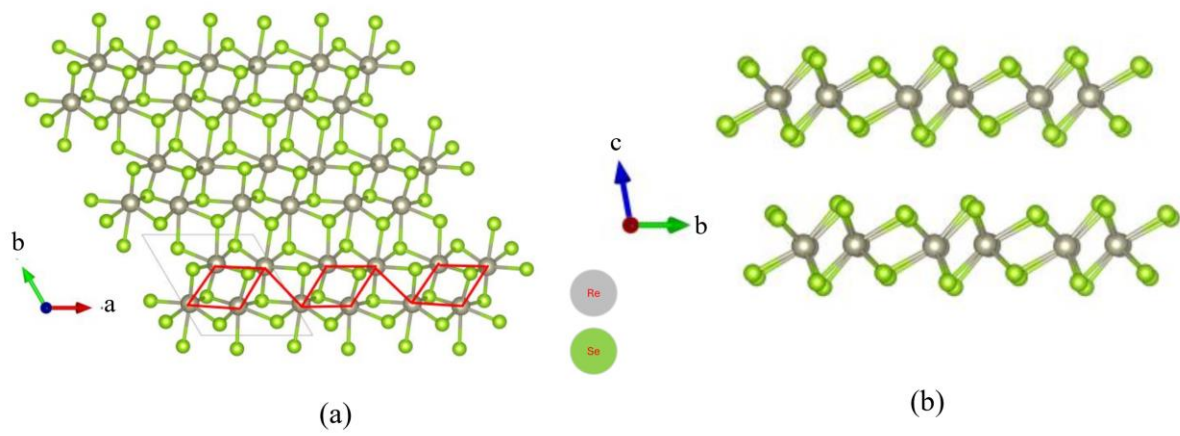


Fig. 1. Onasanya, *et al.*

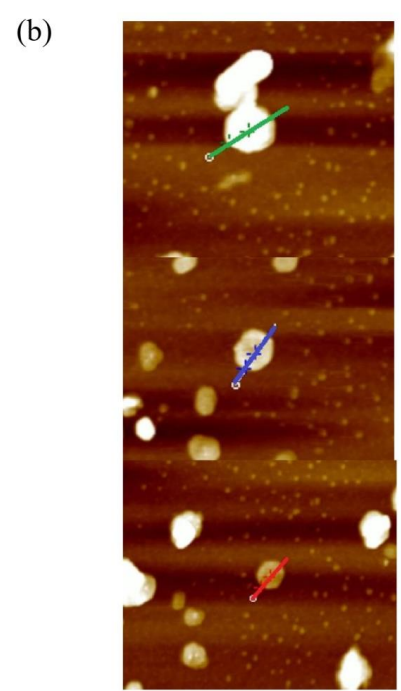
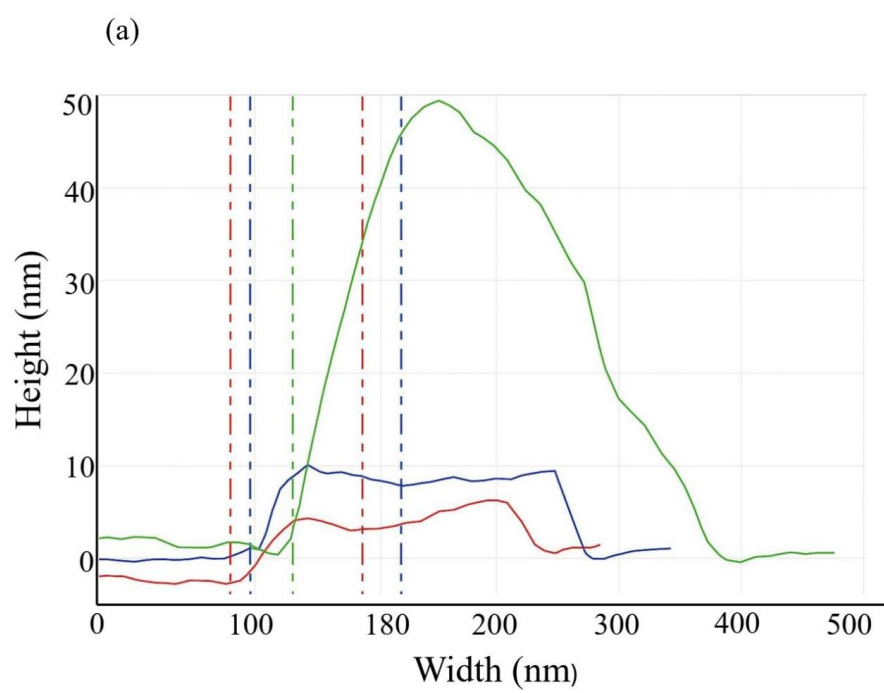
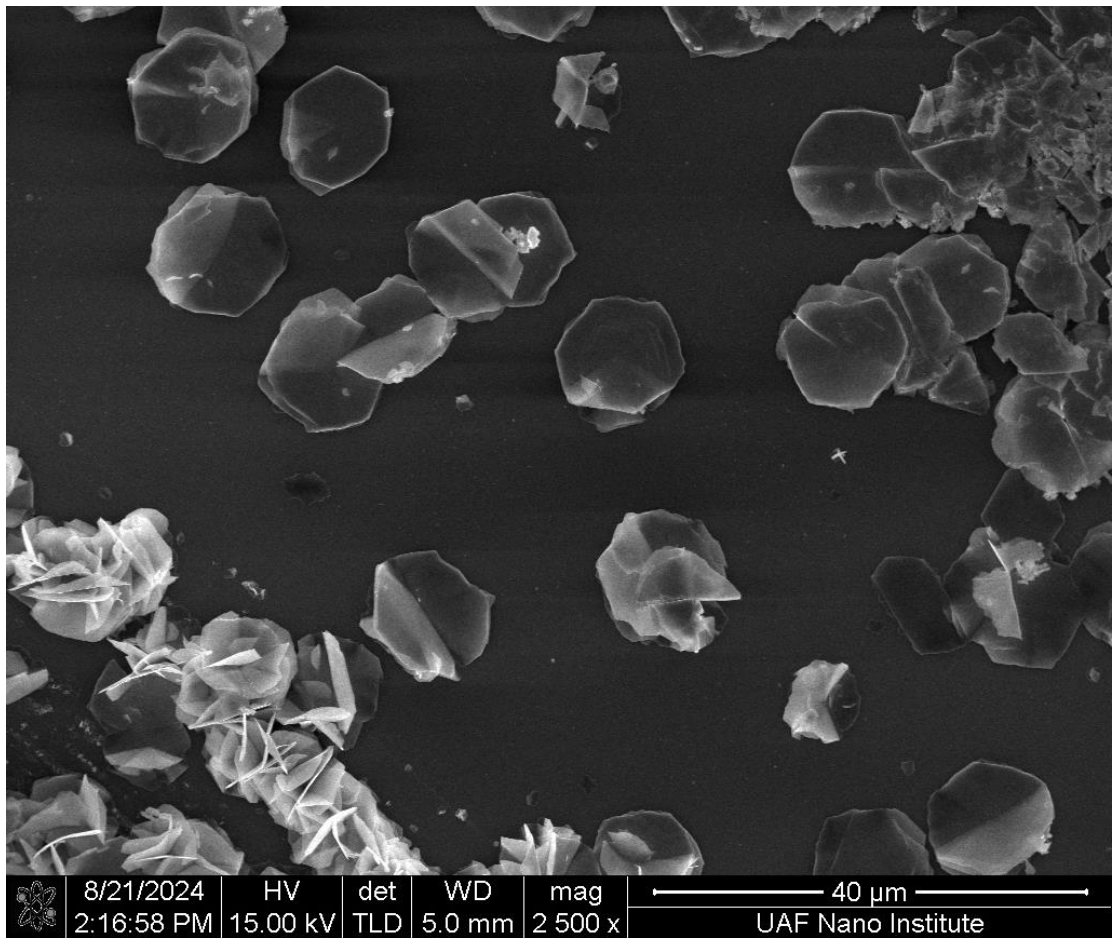


Fig. 2. Onasanya, *et al.*



8/21/2024  
2:16:58 PM

HV  
15.00 kV

det  
TLD

WD  
5.0 mm

mag  
2 500 x

40  $\mu$ m  
UAF Nano Institute

Fig. 3. Onasanya, *et al.*

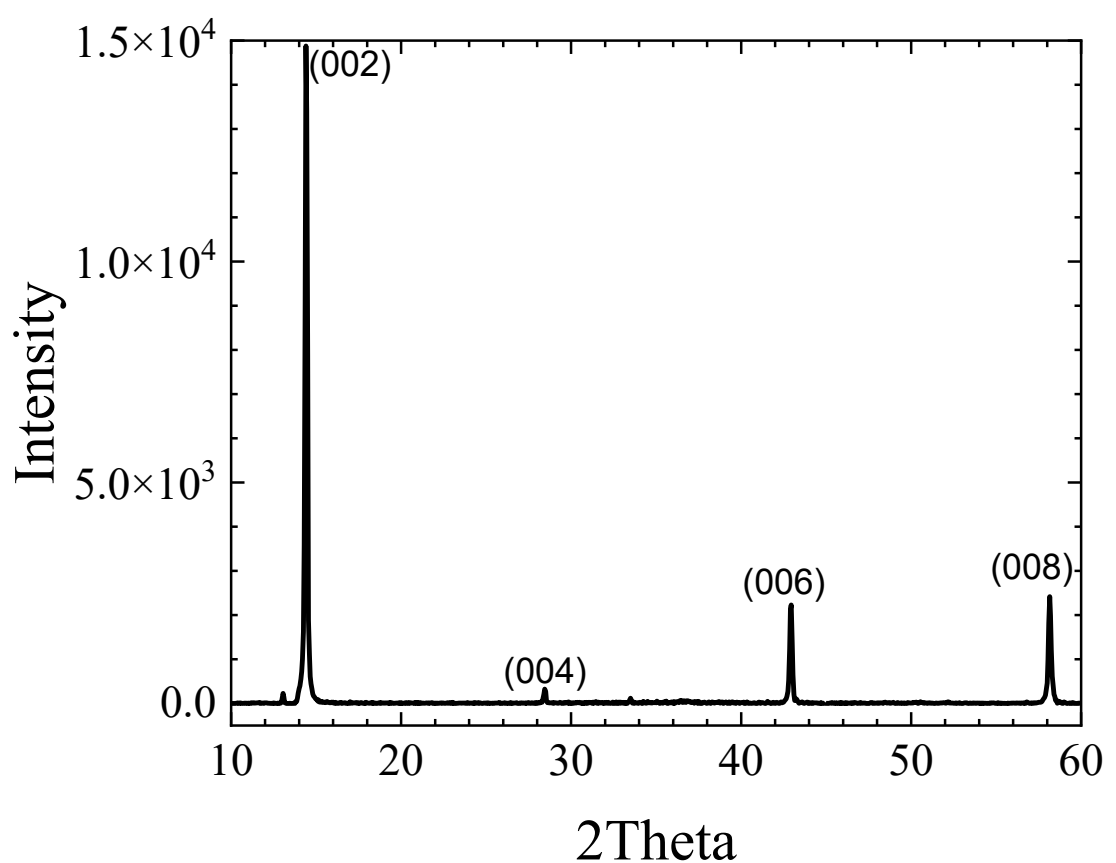


Fig. 4. Onasanya, *et al.*

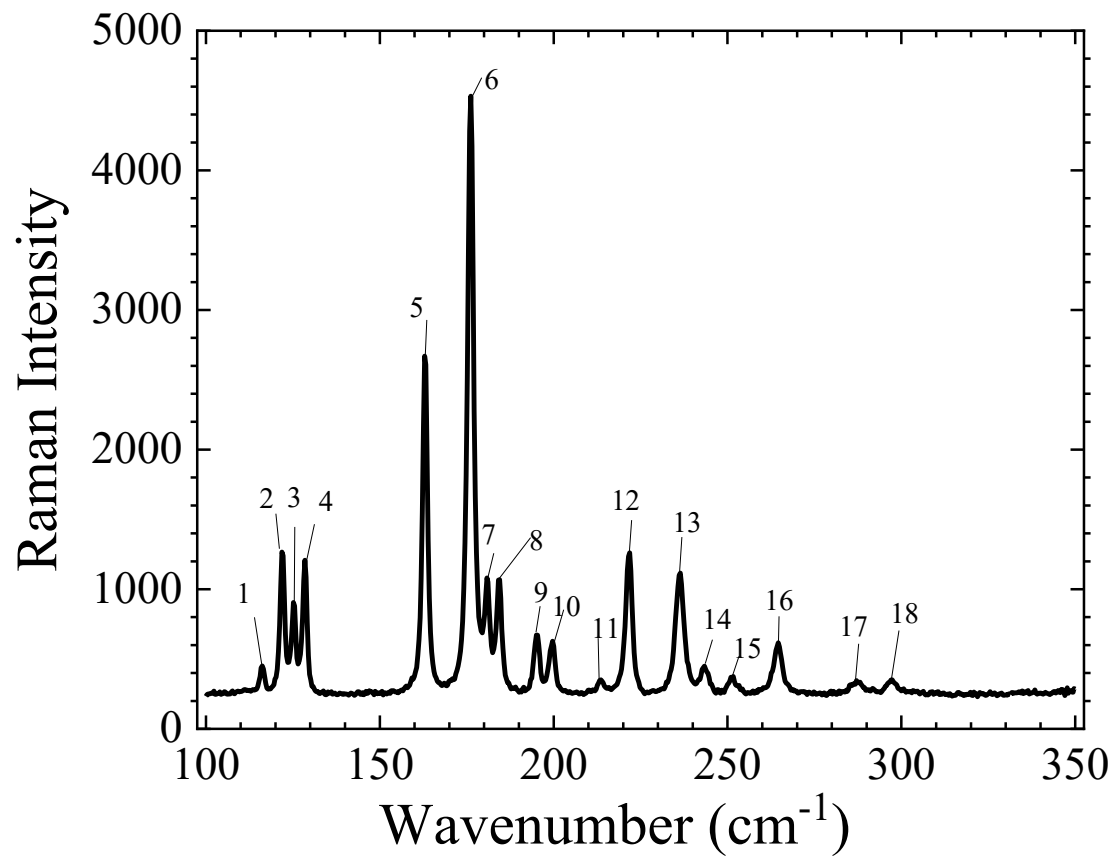


Fig. 5. Onasanya, *et al.*

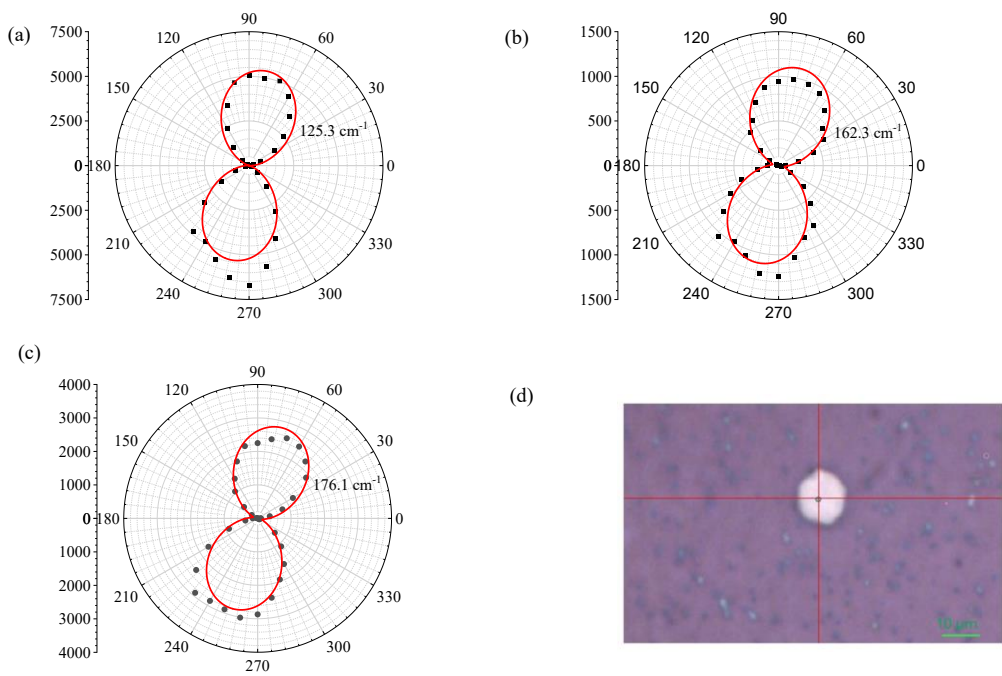


Fig. 6 Onasanya, *et al.*

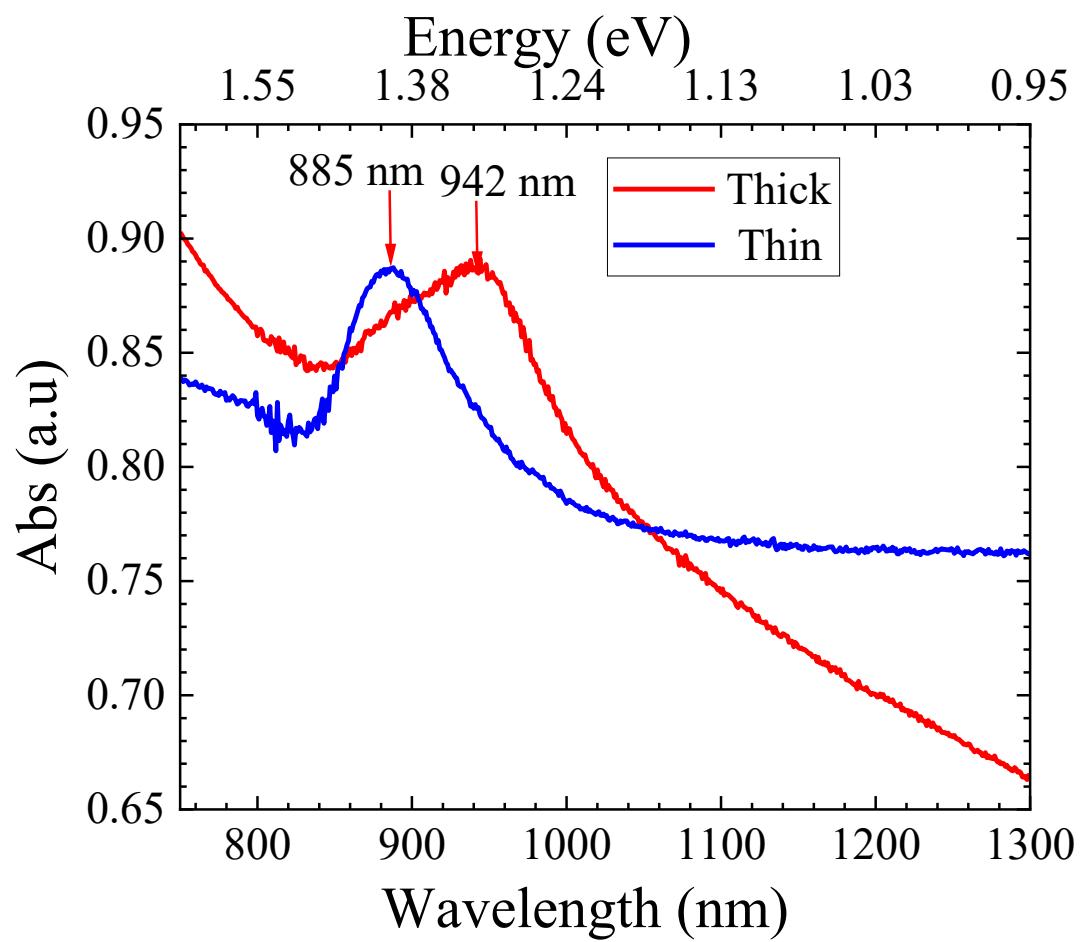


Fig. 7. Onasanya, *et al.*

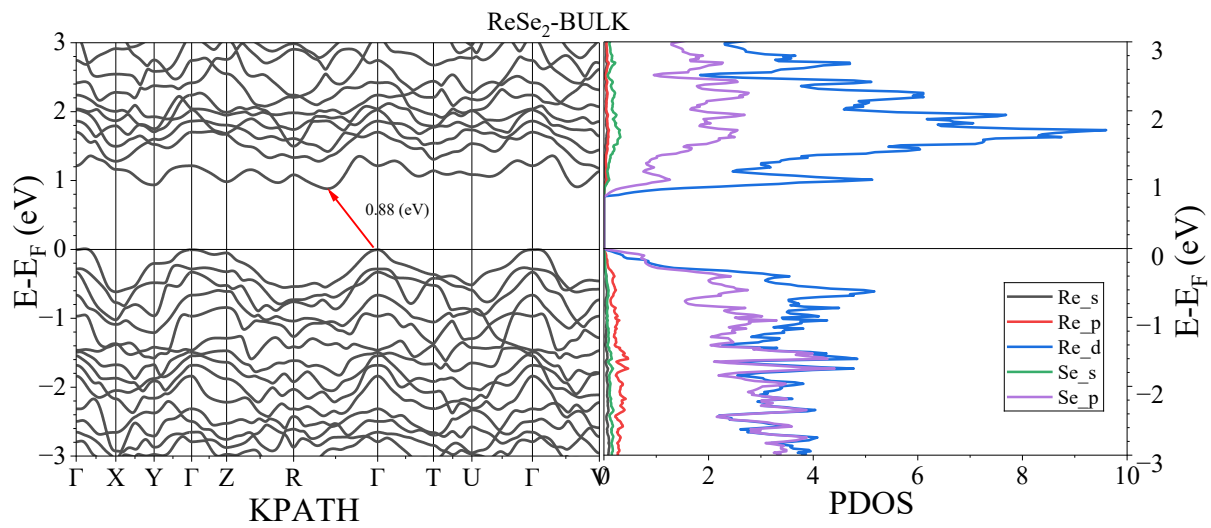


Fig. 8(a). Onasanya, *et al.*

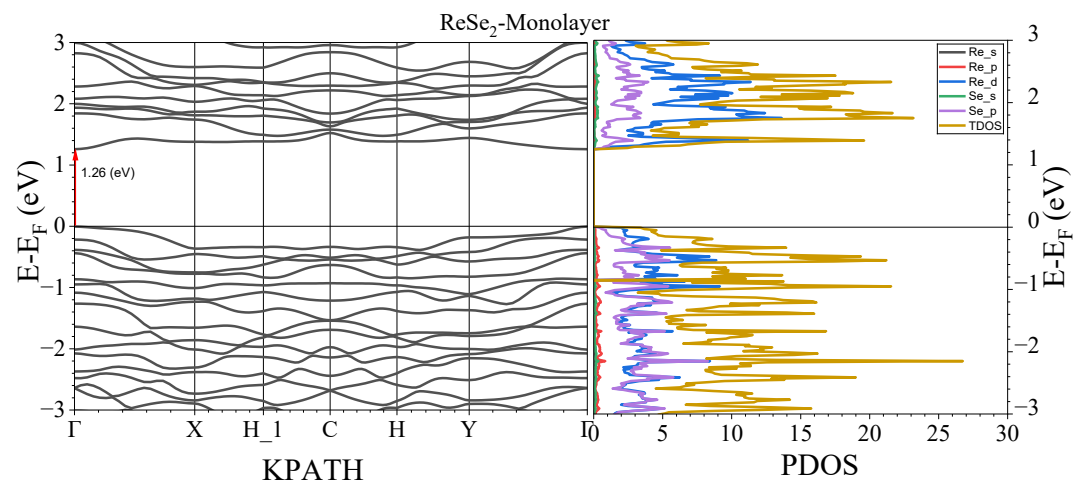


Fig. 8(b). Onasanya, *et al.*

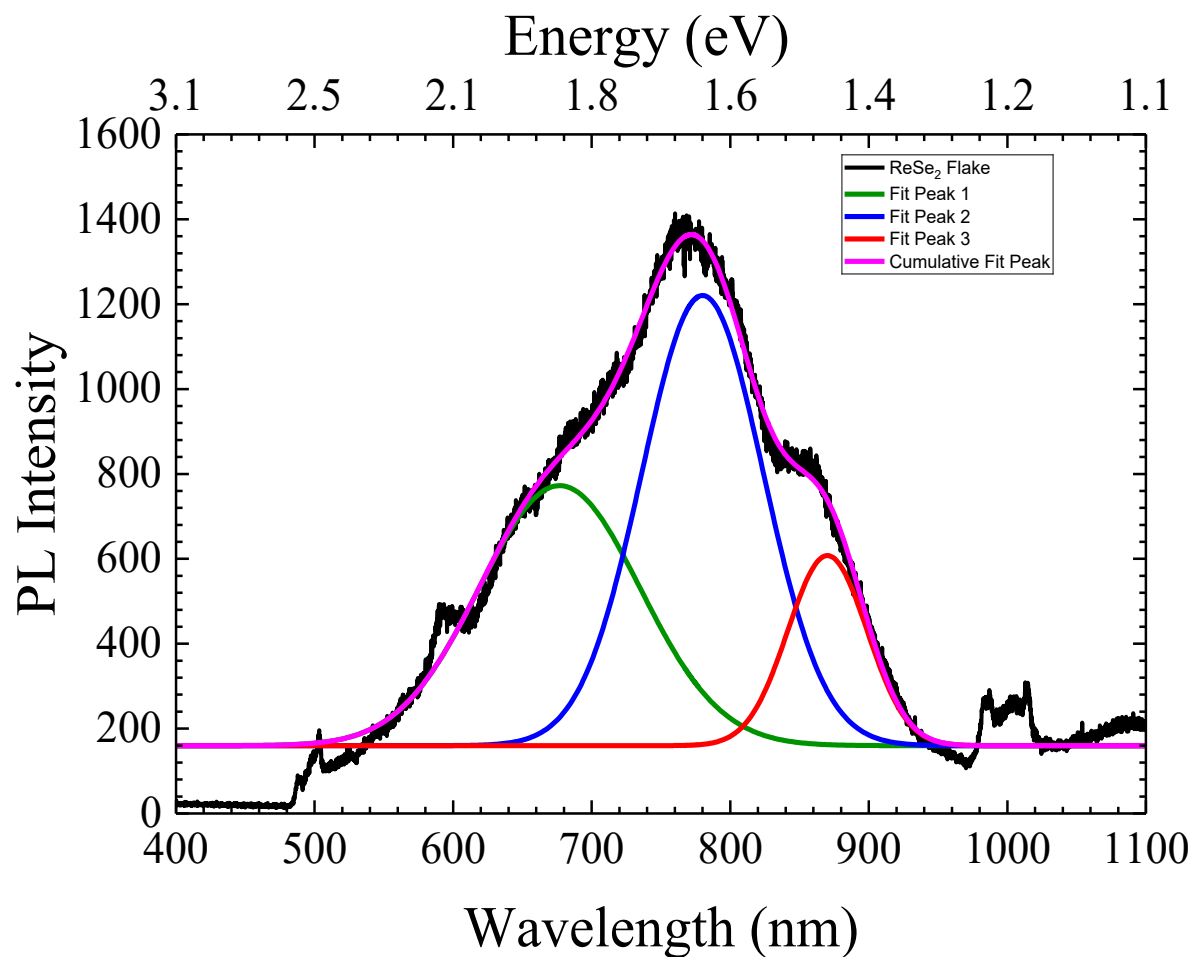


Fig. 9. Onasanya, *et al.*